JURNAL TEKNIK MESIN
INSTITUT TEKNOLOGI PADANG
https://jtm.itp.ac.id/index.php/jtm
Vol. 15, No. 2, October 2025

e-ISSN: 2598-8263
p-ISSN: 2089-4880

Structural Evaluation and Optimization of a Peanut Shelling Machine Frame Using Finite Element Analysis

M. Ibnu Hakim [1], Anrinal Anrinal [2,*],Asmara Yanto [2]
[1] Undergraduated Program of Mechanical Engineering, Institut Teknologi Padang
Jl. Gajah Mada Kandis Nanggalo, Padang, Indonesia
[2] Department of Mechanical Engineering, Institut Teknologi Padang
Jl. Gajah Mada Kandis Nanggalo, Padang, Indonesia

doi.10.21063/jtm.2025.v15.i2.47-55
Correspondence should be addressed to anrinal@itp.ac.id

Article Information

Received:
Augusyt 04, 2025
Revised:
October 06, 2025
Accepted:
October 13, 2025
Published:
October 31, 2025

Abstract

This study investigates the structural integrity of a peanut shelling machine frame with a capacity of 60 kg/hour using Finite Element Analysis (FEA) in SolidWorks. Two configurations of ASTM A36 angle steel profiles—40×40×3 mm and 20×20×3 mm—were evaluated with a frame geometry of 906×600×900 mm. Operational loads were applied to three critical zones with aggregate weights of 82.6 kg, 5.3 kg, and 13.1 kg, respectively. The structural response was assessed through von Mises stress distribution, nodal displacement, and safety factor analysis. Results indicate that the 40×40×3 mm frame exhibits a maximum stress of 37.114 MPa, displacement of 0.2431 mm, and a safety factor of 6.7, while the 20×20×3 mm frame shows a maximum stress of 73.978 MPa, displacement of 0.4521 mm, and a safety factor of 3.4. Both designs satisfy structural safety requirements, maintaining stresses below the material yield strength of 250 MPa and safety factors above the minimum threshold of 2.0. Stress concentrations were predominantly observed at frame corners. While the smaller profile reduces material usage by 50%, it also decreases stiffness by 86%. The findings demonstrate that the 20×20×3 mm configuration is a cost-effective alternative for static loading conditions, whereas the 40×40×3 mm frame provides higher rigidity suitable for potential dynamic load scenarios.

Keywords: Peanut shelling machine; Finite Element Analysis; ASTM A36 steel; Structural integrity; Frame optimization

1. Introduction

Groundnut (peanut) production in many developing regions continues to face significant post-harvest challenges due to limitations in processing technology. Manual dehulling of groundnuts is labor-intensive, time-consuming, and often results in low throughput and inconsistent kernel quality, which negatively impacts production efficiency and economic competitiveness for smallholder farmers [1]. This inefficiency highlights the need for mechanical innovations capable of enhancing operational productivity while maintaining product integrity.

Mechanized groundnut shelling machines with capacities in the range of 60 kg/hour have emerged as promising solutions to address these constraints by reducing manual labor and increasing throughput. Within such machines, the frame structure plays a critical role as the primary load-bearing component that supports all operational parts and ensures overall mechanical stability. Structural failure of the frame may lead to machine malfunction, decreased performance, and increased safety risks during operation [2], [3]. Thus, rigorous validation of frame design through structural analysis becomes essential to guarantee

performance and safety before fabrication and field deployment.

Finite Element Analysis (FEA) has become a widely accepted computational method for evaluating the structural behavior of mechanical components under realistic load conditions. Through numerical simulation, FEA can predict stress distribution, deformation, and safety factors without requiring physical prototypes, thereby saving time and resources in the design phase [4]. In agricultural machinery research, FEA has been successfully applied to assess the structural integrity of various machine components, including tractors, harvesters, and processing equipment frames, demonstrating its effectiveness in identifying critical stress zones and potential failure points [5]–[8].

Despite the proven utility of FEA in structural evaluation across multiple domains, studies that specifically investigate the structural performance of groundnut sheller frames are limited. Past research on design optimization for groundnut processing equipment has predominantly focused on mechanical components or operational parameters rather than comprehensive structural analysis of the support frame [2], [9], [10]. Moreover, existing works often evaluate a single frame configuration without meaningful comparison between alternative structural designs, leaving a gap in optimized frame solutions that balance strength, material efficiency, and cost.

This study employs FEA using SolidWorks Simulation to assess and compare two frame configurations constructed from ASTM A36 low-carbon steel angle profiles—40×40×3 mm and 20×20×3 mm—with overall dimensions of 906 mm (length) × 600 mm (width) × 900 mm (height). Key structural response parameters examined include von Mises stress distribution, nodal displacement, and safety factor, which are fundamental indicators of the frame's ability to withstand static operational loads without failure [4], [5], [11]. By evaluating these parameters, this research aims to validate the existing frame design and explore opportunities for material reduction while maintaining minimum safety requirements.

The primary objectives of this work are to (1) validate the adequacy of the existing groundnut sheller frame under representative operational load conditions through static FEA, (2) assess the feasibility of a reduced profile dimension as a cost-effective alternative, and (3) provide numerically validated design recommendations for mechanically robust and economically viable groundnut sheller frames. The outcomes of this research are expected to contribute to the broader field of agricultural machinery design by offering a rigorous structural analysis framework and practical insights into frame optimization.

2. Materials and Methods

This study employed a computer-aided engineering (CAE) approach using Finite Element Analysis (FEA) to evaluate the structural performance of a groundnut shelling machine frame, enabling detailed investigation of mechanical responses under operational loads without requiring physical prototypes [1]–[3], [12]. The frame was fabricated from ASTM A36 low-carbon steel angle profiles (Table 1), with cross-sectional dimensions of 40×40×3 mm, a modulus of elasticity of 200 GPa, a yield strength of 250 MPa, and a tensile strength of 400–550 MPa [2], [4]. A three-dimensional CAD model was developed in SolidWorks 2023, representing the actual machine geometry with dimensions of 906 mm (length) × 600 mm (width) × 900 mm (height). Two frame configurations were analyzed: the original 40×40×3 mm profile and a reduced 20×20×3 mm profile to explore potential material savings while ensuring structural adequacy.

Table 1. Material Properties of ASTM A36 Steel

Property	Value	Reference
Modulus of Elasticity (E)	200 GPa	[2], [4]
Yield Strength (σ_y)	250 MPa	[2], [4]
Ultimate Tensile Strength	400–550 MPa	[2], [4]
Poisson's Ratio (ν)	0.3	[4]
Density (ρ)	7850 kg/m³	[4]

Operational loads were applied based on actual machine usage at a nominal capacity of 60 kg/hour, distributed across three critical zones (Table 2). Zone 1, encompassing the shelling unit, bearings, hopper, and pulley system, experienced an aggregate load of 82.6 kg. Zone 2, including the prime mover and drive components, was subjected to 5.3 kg, while Zone 3, consisting of the blower, protective casing, and secondary supports, carried 13.1 kg. These loads were modeled as static forces to accurately reflect operational conditions [1], [5], [6].

Table 2. Provides a summary of the applied loads and corresponding components in each zone.

Zone	Components	Load (kg)
1	Shelling unit, bearings, hopper, pulley system	82.6
2	Prime mover (engine) and drive components	5.3
3	Blower, protective casing, secondary supports	13.1

The CAD model was discretized using 3D solid elements, with a mesh size ranging from 2.90 mm in refined regions to 58.17 mm in coarser zones, producing 252,293 elements and 547,321 nodes. A mesh convergence study was conducted to ensure that further refinement did not significantly alter stress, displacement, or safety factor results [12]–[14]. Fixed supports were applied at the frame's base to replicate actual mounting conditions while allowing elastic deformation.

The FEA simulation outputs included von Mises stress distribution, maximum nodal displacement, and safety factor (FoS). Von Mises stress identified regions susceptible to yielding or potential failure, maximum displacement served as a measure of structural stiffness, and the safety factor verified the design against operational loads, with a minimum threshold of 2.0 according to industrial design standards [1], [4], [7], [12]. Collectively, these parameters provided a comprehensive assessment of frame integrity and stiffness under static load conditions.

The overall FEA methodology followed a systematic workflow, illustrated in Figure 1, which ensured methodological rigor and reproducibility. The workflow began with CAD modeling of the frame geometry, followed by assignment of material properties corresponding to ASTM A36 steel. Operational loads and boundary conditions were then applied, after which mesh generation and convergence verification were performed. Static structural analysis was conducted to compute stress, displacement, and safety factor distributions. Results were analyzed to identify critical stress zones, maximum deformations, and areas with insufficient safety margins. Finally, design validation and potential optimization strategies, including reduction of profile dimensions, were evaluated to maintain safety while improving material efficiency. This integrated workflow provided a robust framework for evaluating and optimizing the mechanical performance of groundnut sheller frames prior to physical fabrication, ensuring both structural reliability and cost-effectiveness.

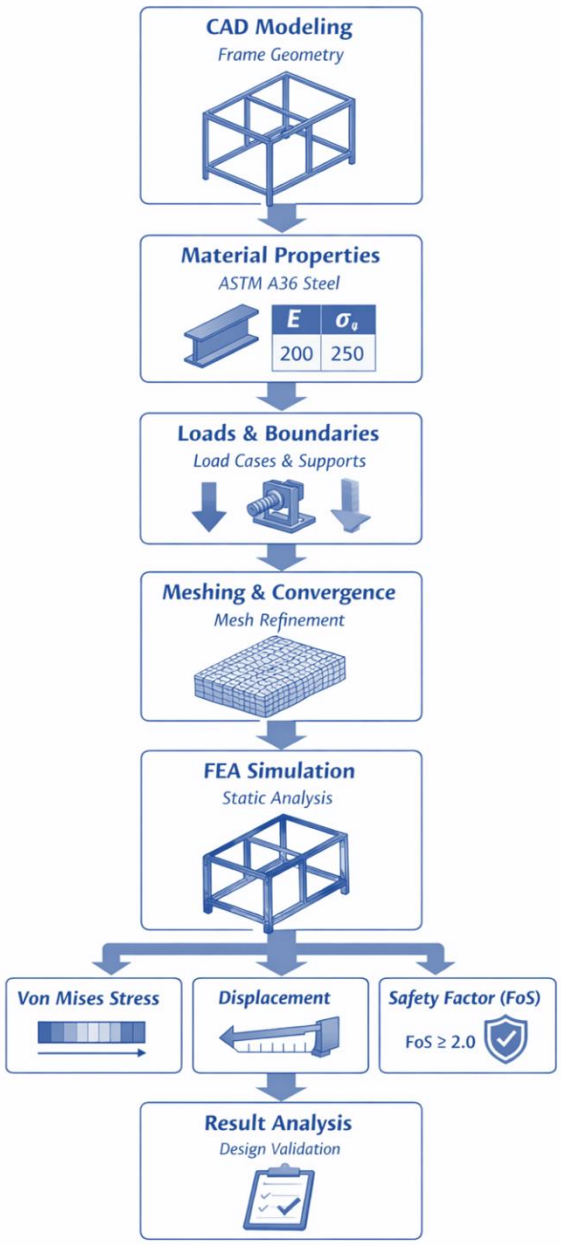

Figure 1. FEA workflow for structural evaluation of the groundnut sheller frame.

3. Results and Discussion

A. Von Mises Stress Distribution under Operational Loads

The structural response of the groundnut sheller frame was evaluated under static operational loading using von Mises stress as the primary criterion for assessing material yielding and potential failure. Von Mises stress provides a scalar measure of the combined principal stresses within the structure, allowing identification of regions susceptible to plastic deformation under applied loads. Two frame configurations were considered: the original 40×40×3 mm profile and a reduced 20×20×3 mm profile, with stress analyses conducted across three operational load zones.

For load zone 1, which includes the shelling unit, bearings, hopper, and pulley system, the 40×40×3 mm frame exhibits a maximum von Mises stress of 37.114 MPa at the frame corners, while the minimum stress occurs at 4.639 MPa in less loaded regions. This stress distribution is visualized in Figure 2, where the red-brown regions indicate areas of peak stress concentration and the light blue regions correspond to minimum stress. The corner concentration results from geometric discontinuities, which amplify local stresses due to the stress concentration effect. Reducing the profile to 20×20×3 mm leads to a notable increase in stress, with a maximum of 73.978 MPa and a minimum of 9.247 MPa, as shown in Figure 3. The comparison clearly demonstrates that halving the cross-section nearly doubles the maximum stress, reflecting reduced structural capacity due to a smaller moment of inertia.

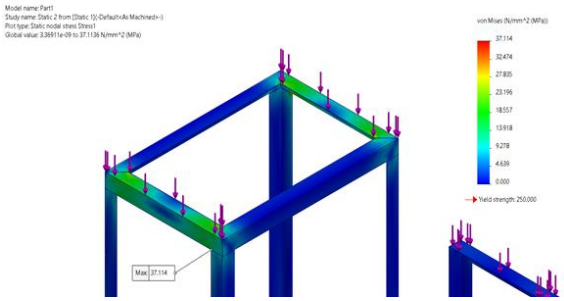

Figure 2. Von Mises stress distribution of the 40×40×3 mm groundnut sheller frame under load zone 1 (shelling unit, bearings, hopper, and pulley system). Maximum stress localized at frame corners is 37.114 MPa.

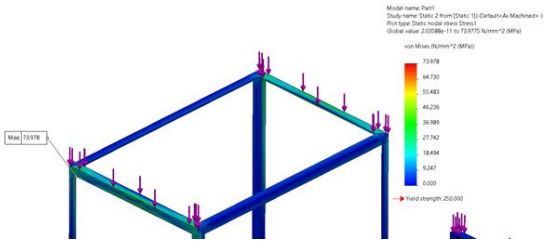

Figure 3. Von Mises stress distribution of the 20×20×3 mm groundnut sheller frame under load zone 1, showing amplified maximum stress of 73.978 MPa at the same corner locations.

In load zone 2, representing the motor and drive components, the stress magnitude is significantly lower. The 40×40×3 mm frame experiences a maximum stress of 2.357 MPa and a minimum of 0.295 MPa, as illustrated in Figure 4. These values suggest that load zone 2 imposes minimal contribution to the overall structural demand. For the 20×20×3 mm configuration, the maximum stress increases to 5.159 MPa with a minimum of 0.645 MPa, as depicted in Figure 5, maintaining the trend of stress amplification due to reduced profile dimensions while remaining far below the yield strength.

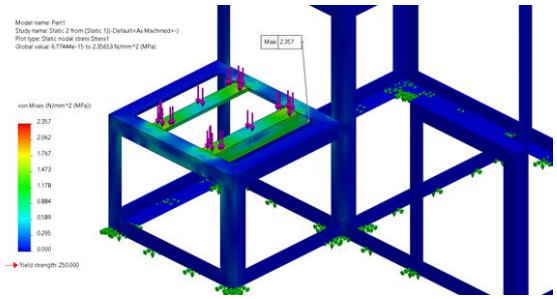

Figure 4. Von Mises stress distribution of the 40×40×3 mm frame under load zone 2 (motor and drive components). Maximum stress is 2.357 MPa, indicating minimal structural demand.

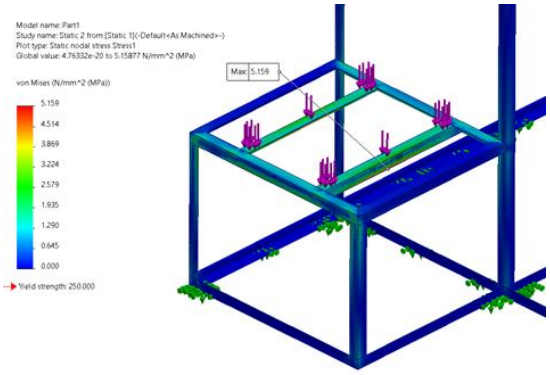

Figure 5. Von Mises stress distribution of the 20×20×3 mm frame under load zone 2, with maximum stress increased to 5.159 MPa due to reduced profile dimensions.

For load zone 3, which includes the blower, protective casing, and auxiliary supports, the 40×40×3 mm frame exhibits a maximum von Mises stress of 4.404 MPa at the corners and a minimum of 0.550 MPa, as shown in Figure 6. The stress distribution illustrates efficient load transfer through the frame's structural paths. The reduced 20×20×3 mm profile, shown in Figure 7, experiences a maximum stress of 8.205 MPa and a minimum of 1.026 MPa, confirming that stress amplification persists across all load zones with smaller profiles.

A direct comparison of maximum von Mises stress between the two frame configurations is presented in Figure 8, which highlights that the 20×20×3 mm frame experiences nearly twice the peak stress of the 40×40×3 mm frame (73.978 MPa vs. 37.114 MPa). Despite this increase, both configurations remain well below

the ASTM A36 yield strength of 250 MPa, indicating a sufficient safety margin. The larger 40×40×3 mm frame demonstrates superior stiffness and more optimal stress distribution, whereas the smaller profile provides material savings at the expense of increased local stress and reduced rigidity.

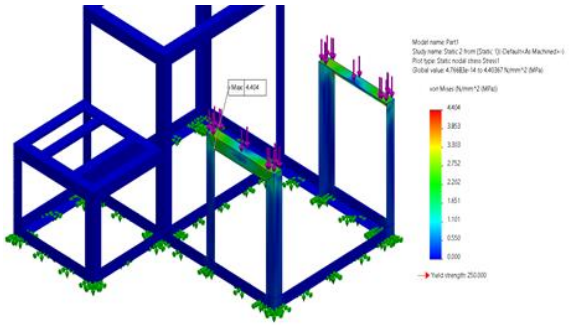

Figure 6. Von Mises stress distribution of the 40×40×3 mm frame under load zone 3 (blower, protective casing, and auxiliary supports). Maximum stress reaches 4.404 MPa at the frame corners.

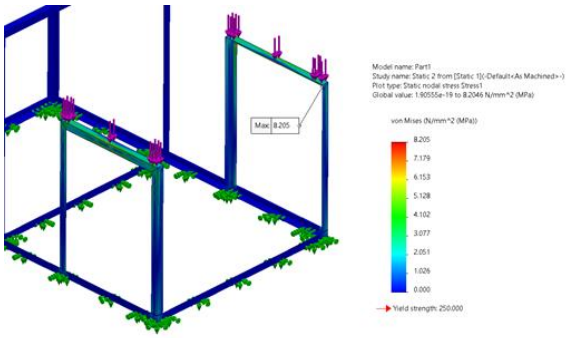

Figure 7. Von Mises stress distribution of the 20×20×3 mm frame under load zone 3, showing maximum stress of 8.205 MPa, highlighting sensitivity to profile reduction.

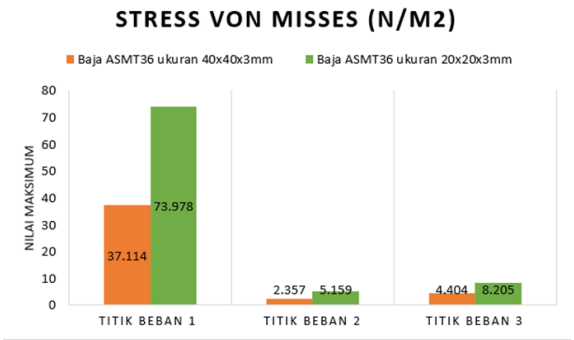

Figure 8. Comparative plot of maximum von Mises stress for 40×40×3 mm and 20×20×3 mm frame configurations across all load zones, illustrating the effect of profile reduction on stress amplification.

The consistent observation of stress concentration at frame corners across all loading conditions emphasizes the critical role of geometric design in mitigating localized overstress. These insights suggest that fillets or corner reinforcements could further enhance structural reliability, particularly when considering reduced profile designs for cost-effective production.

B. Structural Displacement under Operational Loads

Structural displacement analysis was conducted to evaluate the elastic deformation of the groundnut sheller frame under operational loading conditions. Displacement serves as a direct measure of structural stiffness, and excessive deflection may compromise dimensional accuracy and overall machine performance.

Load Zone 1

The resultant displacement of the 40×40×3 mm frame under load zone 1, which includes the shelling unit, bearings, hopper, and pulley system, is presented in Figure 9. The maximum displacement was recorded at 0.2431 mm, localized at the central region of the frame, while the minimum displacement of 0.0243 mm occurred near the fixed supports. The displacement pattern exhibits a beam-like deflection consistent with classical structural theory. Reducing the profile dimension to 20×20×3 mm significantly increased deformation, as shown in Figure 10, with a maximum displacement of 0.4521 mm and a minimum of 0.0452 mm, indicating an 86 % reduction in stiffness relative to the original frame.

Load Zone 2

For load zone 2, which accounts for the motor and drive components, the 40×40×3 mm frame experienced minimal displacement, as illustrated in Figure 11. The maximum deflection was 0.0171 mm with a minimum of 0.0034 mm, suggesting that this load contributes marginally to overall structural deformation. The reduced 20×20×3 mm frame displayed proportionally higher displacement (maximum 0.0395 mm, minimum 0.0040 mm), as shown in Figure 12, maintaining a consistent trend of amplified deflection due to reduced cross-sectional rigidity.

Load Zone 3

Load zone 3, which includes the blower, protective casing, and auxiliary supports, produced moderate deflection in the 40×40×3 mm frame, with a maximum displacement of 0.0309 mm and a minimum of 0.0031 mm at the central structure, as shown in Figure 13. The reduced 20×20×3 mm frame exhibited a maximum displacement of 0.0615 mm and a minimum of 0.0062 mm, confirming the consistent sensitivity of frame stiffness to cross-sectional reduction (Figure 14).

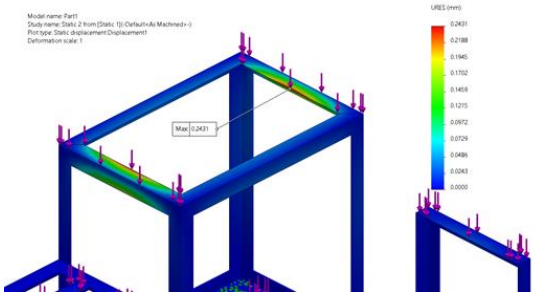

Figure 9. Resultant displacement distribution of the 40×40×3 mm frame under load zone 1 (shelling unit, hopper, bearings, and pulley system). Maximum displacement occurs at the central region.

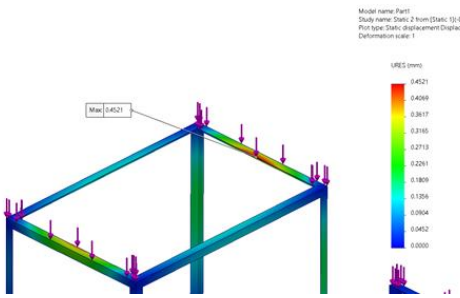

Figure 10. Resultant displacement distribution of the 20×20×3 mm frame under load zone 1, showing increased deformation compared to the 40×40×3 mm frame.

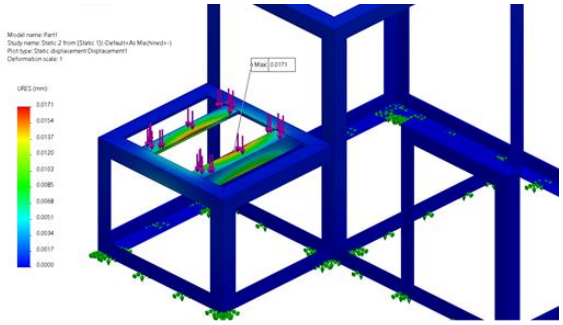

Figure 11. Displacement distribution of the 40×40×3 mm frame under load zone 2 (motor and drive components). The maximum displacement is minimal, indicating low contribution of this load zone to overall deflection.

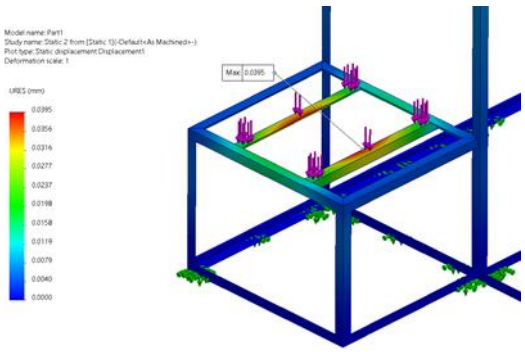

Figure 12. Displacement distribution of the 20×20×3 mm frame under load zone 2, showing proportional increase in maximum displacement due to reduced frame rigidity.

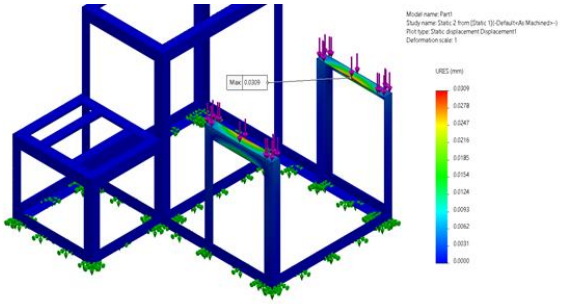

Figure 13. Displacement distribution of the 40×40×3 mm frame under load zone 3 (blower, protective casing, and auxiliary supports). Moderate deflection is observed.

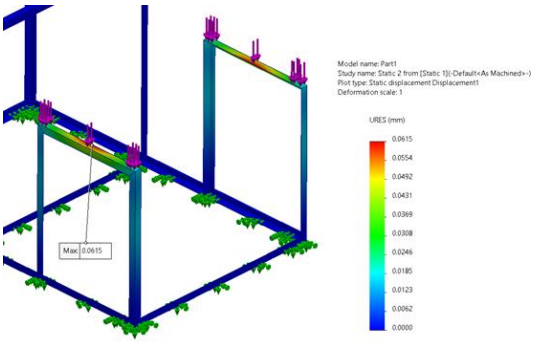

Figure 14. Displacement distribution of the 20×20×3 mm frame under load zone 3, demonstrating amplified maximum displacement consistent with trends in previous load zones.

Comparative Analysis

A comparative summary of maximum displacements across all load zones for both frame configurations is presented in Figure 15. The 20×20×3 mm frame shows a maximum displacement of 0.4521 mm, nearly double that of the 40×40×3 mm frame (0.2431 mm) under load zone 1. Although displacements in both configurations remain within acceptable tolerances for static operation, the larger 40×40×3 mm profile demonstrates superior rigidity, which is advantageous for maintaining long-term operational stability and precision.

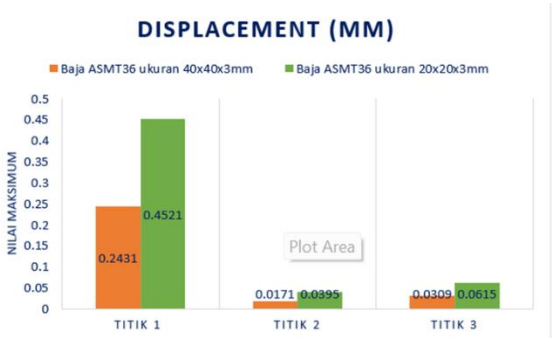

Figure 15. Comparative graph of maximum displacement for 40×40×3 mm and 20×20×3 mm frames across all load zones, highlighting the superior stiffness of the larger frame configuration.

C. Safety Factor Analysis

The factor of safety (FoS) represents the ratio of material strength to actual operational stress and serves as a fundamental parameter for validating structural reliability. Industrial machinery design standards typically require a minimum FoS of 2.0 to ensure adequate safety margins against unexpected loads and material variability.

For the original 40×40×3 mm frame configuration, the simulation results indicate a minimum FoS of 6.7, as shown in Figure 16. This high safety margin demonstrates that the structure can sustain operational loads with substantial reserve capacity, providing confidence in long-term structural reliability and resilience to potential overloading or material degradation during service life.

Reducing the frame profile to 20×20×3 mm results in a lower FoS, as presented in Figure 17, with a minimum value of 3.4. While this configuration still exceeds the minimum design threshold of 2.0, the reduced margin indicates limited capacity to accommodate dynamic loads, impact events, or material property deterioration due to corrosion or fatigue over extended operation.

A comparative analysis of the FoS between the two frame configurations is summarized in Figure 18. The larger 40×40×3 mm frame exhibits a FoS of 6.7, significantly higher than the 3.4 of the 20×20×3 mm frame. This difference highlights a trade-off between material efficiency and structural robustness. While the larger frame provides potential over-design suitable for optimization, the smaller frame approaches the minimum acceptable design limit, emphasizing the need for careful consideration of operational loading scenarios when selecting a cost-effective yet reliable frame configuration.

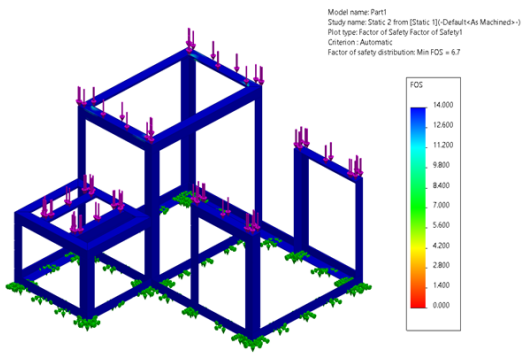

Figure 16. Factor of safety distribution for the 40×40×3 mm frame, showing a minimum value of 6.7, indicating high structural reliability under operational loads.

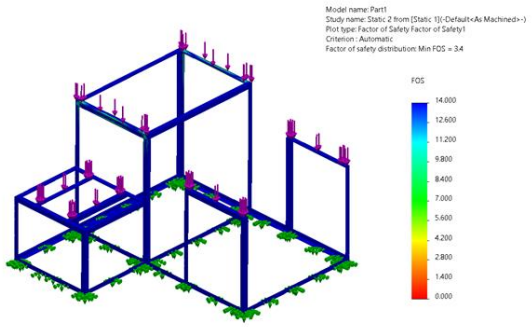

Figure 17. Factor of safety distribution for the 20×20×3 mm frame, showing a minimum value of 3.4, which remains above the design threshold of 2.0.

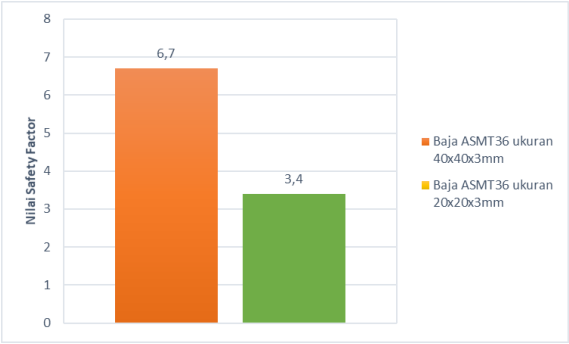

Figure 18. Comparative chart of minimum factor of safety between 40×40×3 mm and 20×20×3 mm frame configurations, highlighting the trade-off between material efficiency and structural robustness.

D. Comparative Discussion of Frame Configurations

A comparative evaluation of the two frame configurations-40×40×3 mm and 20×20×3 mm-reveals clear trade-offs between structural performance and material efficiency under static operational loads. The 40×40×3 mm frame consistently exhibits lower von Mises stress, smaller displacements, and higher safety factors across all applied load zones, indicating superior stiffness and robustness. Specifically,

the maximum stress under the primary load zone is 37.114 MPa for the 40×40×3 mm frame, less than half of the 73.978 MPa observed in the reduced 20×20×3 mm frame (Figures 2–3, 8). The stress concentration remains predominantly localized at corner junctions for both configurations, highlighting geometric discontinuities as critical regions for structural attention.

The displacement results corroborate these observations. The 40×40×3 mm frame demonstrates a maximum resultant displacement of 0.2431 mm under the primary load, whereas the 20×20×3 mm frame exhibits 0.4521 mm, reflecting an 86 % reduction in stiffness (Figures 9–10, 15). Despite the increase in displacement for the smaller profile, both configurations remain within acceptable tolerances for static operation, ensuring dimensional integrity and operational functionality.

Factor of safety analysis further emphasizes the performance disparity. The 40×40×3 mm frame maintains a minimum FoS of 6.7, providing a substantial margin against material yielding and unexpected overloads. In contrast, the 20×20×3 mm frame records a minimum FoS of 3.4, which, while above the industry threshold of 2.0, indicates a narrower safety margin that may limit resilience under dynamic or impact loads (Figures 16–18).

Overall, the comparative assessment demonstrates that the 20×20×3 mm frame configuration can serve as a cost-effective alternative for applications where static loading predominates and material savings are a priority, achieving a 50 % reduction in steel usage. However, the 40×40×3 mm frame provides superior structural performance with enhanced stiffness and higher safety margins, making it more suitable for operational scenarios that may involve dynamic effects, unexpected loading, or long-term fatigue considerations. This integrated analysis underscores the critical balance between material efficiency, cost, and structural reliability in the design optimization of agricultural machinery frames.

4. Conclusion

This study conducted a comprehensive structural evaluation of a groundnut sheller frame using Finite Element Analysis (FEA) in SolidWorks. Two frame configurations, 40×40×3 mm and 20×20×3 mm ASTM A36 angle steel profiles, were analyzed under operational loads distributed across three critical zones. The assessment focused on von Mises stress distribution, nodal displacement, and factor of safety as key indicators of structural integrity and stiffness.

The results demonstrate that both frame configurations satisfy structural safety requirements, with maximum von Mises stresses well below the material yield strength of 250 MPa and safety factors exceeding the minimum design threshold of 2.0. The 40×40×3 mm frame exhibited superior rigidity, lower displacement (0.2431 mm under load Zone 1), and a higher factor of safety (6.7), indicating a robust structural performance capable of accommodating potential dynamic loads and long-term operational variability. In contrast, the 20×20×3 mm frame, while maintaining an acceptable safety factor of 3.4, displayed higher stress concentrations, increased maximum displacement (0.4521 mm under load Zone 1), and reduced stiffness by 86% relative to the larger profile, representing a trade-off between material efficiency and structural robustness.

The comparative analysis highlights that the 20×20×3 mm configuration provides a cost-effective alternative for static loading conditions, reducing material usage by approximately 50% without compromising basic operational safety. Meanwhile, the 40×40×3 mm frame offers a conservative design with higher safety margins, suitable for applications where dynamic loading, impact, or long-term fatigue may be critical considerations.

Overall, this study validates the structural adequacy of the existing groundnut sheller frame, provides insights into the effects of profile dimension reduction, and offers numerically supported recommendations for frame optimization. The findings contribute to the development of mechanically robust and economically viable agricultural machinery by establishing a rigorous framework for pre-fabrication structural evaluation and design improvement.

Acknowledgements

Thank you to all the Mechanical Engineering Staff of the Padang Institute of Technology who have contributed so that this article can be completed.

References

[1] E. I. Nwankwo, "Performance Evaluation Of Small-Scale Groundnut Decorticators: A Comprehensive Review," Agric. Eng. Today, vol. 32, no. 2, pp. 85–102, 2025.

[2] E. Wahyudi and H. Mahmudi, "Desain Rangka Alat Pengupas Kulit Kacang Tanah Dengan Kapasitas 30kg/Jam," J. Teknol. Pertan., vol. 8, pp. 1–11, 2024.

[3] B. Badruzzaman, T. Endramawan, M. Rahmi, and J. Susandi, "Analisis Kekuatan Pembebanan Rangka Pada Perancangan Mesin Grading Fish Jenis Ikan Lele Menggunakan Simulasi SolidWorks," in Proc. Ind. Res. Work. Natl. Semin., vol. 11, no. 1, pp. 259–262, 2020.

[4] B. T. Chandru and P. M. Suresh, "Finite Element and Experimental Modal Analysis of Car Roof with and without Damper," Mater. Today Proc., vol. 4, pp. 11237–11244, 2022.

[5] M. Fahmi, A. Armila, and R. K. Arief, "Analisis Kekuatan Rangka Mesin Pengupas Kulit Kopi Menggunakan Software SolidWorks Dengan Metode Elemen Hingg," J. Mesin., vol. 1, no. 3, pp. 65–76, 2022.

[6] C. Soolany et al., "Analisis Kekuatan Rangka Mesin Pengupas Kulit Ari Kacang Tanah Tipe Roller Tunggal dengan Evaluasi Material Berstandar Food Grade Menggunakan Simulasi SolidWorks," Maj. Ilm. Momentum, vol. 21, no. 1, pp. 16–20, 2025, doi:10.36499/jim.v21i1.12199.

[7] F. A. Rahman and W. Waskito, "Rancang Bangun dan Analisis Rangka Traktor Pemanen Jagung," Asian J. Sci. Technol. Eng. Art, vol. 1, no. 1, pp. 122–134, 2023, doi:10.58578/ajstea.v1i1.1870.

[8] A. Halim et al., "Analisis Struktur Rangka Box Fermentasi Biji Kakao Menggunakan Metode Elemen Hingga," J. Rekayasa Mesin, vol. 20, no. 1, pp. 6092, 2025, doi:10.32497/jrm.v20i1.6092.

[9] R. A. M. Napitupulu, C. S. P. Manurung, and S. Sihombing, "Perencanaan Daya Dan Perbedaan Jenis Bantalan (Bearing) Pada Mesin Pengupas Kulit Kacang Tanah Kapasitas 60 Kg/Jam," vol. 5, no. 2, pp. 86–94, 2024.

[10] E. Satrya and R. Abu, "Planning of Peanut Skin Peeler Machine Capacity 800 kg/hour," no. 26, pp. 63–78, 2022.

[11] X. Liao et al., "Optimization of a Low-Loss Peanut Mechanized Shelling Technology Based on Moisture Content, Flexible Materials, and Key Operating Parameters," Int. J. Agric. Technol. Eng., pp. 1–29, 2025.

[12] R. Kurowski, "Finite Element Analysis (FEA) fundamentals and discretization," Int. J. Numer. Methods Eng., vol. 24, no. 2, pp. 337–357, 2025, doi:10.33552/GJES.2025.12.000786.

[13] "Mesh Convergence Test Using Finite Element Analysis (FEA) in Shaft Loading," J. Rekayasa Mesin, vol. 15, no. 3, pp. 1271–1280, 2024, doi:10.21776/jrm.v15i3.1516.

[14] M. Hotma et al., "Practical guidelines for mesh convergence in finite element analysis," accessed 2025. [Online]. Available: https://josephwebb.net/mesh_convergence_studies_in_fea.html